This is a repository copy of *Experimental investigation using demountable steel-concrete composite reduced web section (RWS) connections under cyclic loads*.

White Rose Research Online URL for this paper:
https://eprints.whiterose.ac.uk/209858/

Version: Published Version

Article:
Almutairi, F.F., Tsavdaridis, K.D. orcid.org/0000-0001-8349-3979, Alonso-Rodriguez, A. et al. (1 more author) (2024) Experimental investigation using demountable steel-concrete composite reduced web section (RWS) connections under cyclic loads. Bulletin of Earthquake Engineering, 22 (3). pp. 1081-1110. ISSN 1570-761X

https://doi.org/10.1007/s10518-023-01802-y

Reuse
This article is distributed under the terms of the Creative Commons Attribution (CC BY) licence. This licence allows you to distribute, remix, tweak, and build upon the work, even commercially, as long as you credit the authors for the original work. More information and the full terms of the licence here: https://creativecommons.org/licenses/

Takedown
If you consider content in White Rose Research Online to be in breach of UK law, please notify us by emailing eprints@whiterose.ac.uk including the URL of the record and the reason for the withdrawal request.

eprints@whiterose.ac.uk
https://eprints.whiterose.ac.uk/

Bulletin of Earthquake Engineering (2024) 22:1081–1110
https://doi.org/10.1007/s10518-023-01802-y

ORIGINAL ARTICLE

Experimental investigation using demountable steel-concrete composite reduced web section (RWS) connections under cyclic loads

Fahad Falah Almutairi[1] · Konstantinos Daniel Tsavdaridis[2] · Andres Alonso-Rodriguez[3] · Iman Hajirasouliha[4]

Received: 27 May 2023 / Accepted: 15 October 2023 / Published online: 20 November 2023
© The Author(s) 2023

Abstract
This paper presents an experimental study of demountable steel-concrete composite reduced web section (RWS) connections for use in seismic areas. Four composite connection specimens were subjected to sagging and hogging moments to investigate the performance of RWS connections under reversible actions. For such purpose, a single web opening was created near the beam-column joint. Focus was made on the effects of perforation location and composite beam-slab action induced by bolted shear studs within the protected zone. Results indicate that employing RWS connections for seismic retrofit is a viable solution capable of achieving a performance similar to that observed for RBS connections in new buildings. Notably, a Vierendeel Mechanism is formed, allowing for plasticity development in the beam. All RWS connections were capable of achieving an interstory drift larger than 4%, thereby complying with the performance targets set by ANSI/AISC 358-16, ANSI/AISC 341-16 and EC8. Moreover, the deformation of beam-slab shear-transfer bolts was small enough to allow for disassembly after the tests, indicating that the proposed solution could enable reuse and post-earthquake retrofitting.

Keywords Experimental tests · RWS connections · Composite action · Demountable slabs · Cyclic loading · Retrofit

✉ Konstantinos Daniel Tsavdaridis
konstantinos.tsavdaridis@city.ac.uk

[1] School of Civil Engineering, Faculty of Engineering and Physical Sciences, University of Leeds, Woodhouse Lane, Leeds LS2 9JT, UK

[2] Department of Engineering, School of Science and Technology, City, University of London, Northampton Square, London EC1V 0HB, UK

[3] Faculty of Environment, Science and Economy, Department of Engineering, University of Exeter, Streatham Campus, Northcote House, Exeter EX5 4QJ, UK

[4] Department of Civil and Structural Engineering, The University of Sheffield, Sheffield S10 2TN, UK

1 Introduction

Slabs laid over steel girders can improve their structural behaviour, as they enhance stiffness and provide restraint against torsion and out-of-plane instability. However, they usually lead to high strain demands on the beam's bottom flange; whilst there is unsymmetric moment capacity (Kim et al. 2004). By that means, efforts have been made to mitigate this undesirable behaviour; as it could cause brittle failure if the contribution of the composite slab is neglected in the design process (Roeder 2002). Reduced web section (RWS) connections have been proven to act as a ductile fuse with acceptable behaviour under different types of loading while limiting structural instability and protecting non-ductile elements. (Yang et al. 2009; Tsavdaridis et al. 2014, 2021; Shin et al. 2017a, b; Shaheen et al. 2018; Zhang et al. 2019; Davarpanah et al. 2020; Erfani et al. 2020; Bi et al. 2021; Dong et al. 2021; Du et al. 2021; Jia et al. 2021; Lin et al. 2021; Tabar et al. 2022). Testing of RWS connections under monotonic loading (Jia et al. 2021), cyclic load with and without an axial force on the column (Shin et al. 2017a; Zhang et al. 2019; Bi et al. 2021; Tsavdaridis et al. 2021), pseudo-dynamic (Yang et al. 2009), and column removal (Lin et al. 2021, 2022), has demonstrated their ability to develop plasticity at the web opening and facilitate the implementation of the strong column-weak beam framework.

Regulations suggest isolating the slab over protected zones by limiting joint engagement there (CEN 2005a; ANSI/AISC 341-16 2016; ANSI/AISC 358-16 2016). This prevents plastic actions on non-ductile elements of the joint and precludes out-of-plane instability (Civjan et al. 2000, 2001; Jones et al. 2002; Sumner and Murray 2002; Zhang and Ricles 2006a, b; Lee et al. 2016; Di Benedetto et al. 2020). Moreover, such provisions limit the upward shift of the neutral axis, which in turn addresses the concerns about the unsymmetric behaviour of the beam when subjected to sagging moments (bottom flange under tension) (Chen and Chao 2001; Chen et al. 2001; Kim et al. 2004). A recent computational investigation (Almutairi et al. 2023) on composite RWS connections found that such provisions could lead to symmetric moment capacity and simplify the prediction of their ultimate load and deformation capacity. However, the presence of welded shear studs over the protected zone could compromise the attainment of the strong column-weak beam framework. It could strengthen the connection rather than weaken it if composite action is not properly accounted for. This is consistent with the findings of Shaheen et al. (2018) who examined only composite RWS connections with joint action with the slab over the opening. Their study concluded that small to medium web opening sizes should be considered as large beam web openings compromise their stable hysteretic response. However, there is a knowledge gap regarding the effect of the presence of shear studs (bolted or/and welded) over the web opening (protected/plastic zone) on cyclic performance of steel-concrete composite RWS connections.

The use of bolted shear studs could overcome the obstacle of replacing damaged beams in the aftermath of moderate earthquakes. Albeit they are not as ductile as other shear transfer solutions, they keep their integrity and impede extensive deformation of the contact between slab and beam. Hence, such demountable bolts have been introduced as practical alternatives to traditional solutions for facilitating beam decoupling from slabs, and enabling reuse (Moynihan and Allwood 2014; Ataei et al. 2016, 2017, 2019; Liu et al. 2017; Yang et al. 2018; Sencu et al. 2019; Girão Coelho et al. 2020; Chiniforush et al. 2021) (see Fig. 1). The combination of structural fuses, namely RWS, bolted end-plate connections (Tartaglia et al. 2019), and bolted shear studs may provide a cost-effective structural system for speedy seismic rehabilitation. Henceforth, one of the goals of this study is to assess

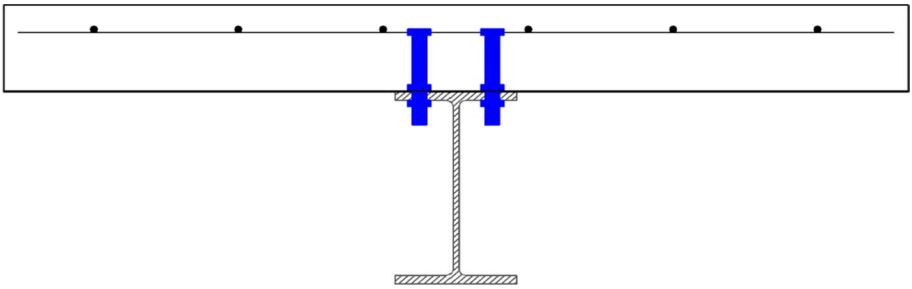

Fig. 1 Demountable bolted shear studs

if the provision of bolts to connect beams and slabs is robust enough to prevent extensive deformation of the beam/slab contact and allow for practical separation of both elements during the replacement of damaged parts whilst temporary support is provided.

The present work extends work done by Almutairi et al. (2023) and Shaheen et al. (2018) that showcased the potential of such structural fuses and their suitability for seismic applications. This paper goes a step further by experimentally investigating the effects of the presence of bolted shear studs on the cyclic behaviour of composite RWS connections, aiming to augment available data to expand on the current status quo. Additionally, the incorporation of RWS into extended end-plate connection is examined for rehabilitation purposes. To achieve this, an extended end-plate connection with a solid-webbed beam was tested under cyclic loading. Subsequently, a web opening was cut into it and the connection specimen was re-tested to simulate the effects of moderate seismicity and demountability of such a combination of structural fuses. The above process is a practical rehabilitation technique for existing steel frames with solid-webbed beams.

2 Behaviour of reduced web section (RWS) connections

The Vierendeel Mechanism (VM) is a highly ductile and stable yield mechanism that occurs in steel perforated beams (i.e., cellular, castellated, etc.) and consequently in RWS connections. This results in the redistribution of global actions to prevent plastic deformation in non-ductile elements (Tsavdaridis and Papadopoulos 2016; Shin et al. 2017a; Tsavdaridis et al. 2017). This load redistribution enhances the rotational capacity and ductility of connections by the formation of plastic hinges (Yang et al. 2009; Tsavdaridis et al. 2014; Erfani and Akrami 2017). Figure 2 illustrates the global and local forces acting around the web opening. The plastic hinges always form in the low moment side (LMS) (where the edge of a web opening is subjected to a lower primary moment) before the high moment side (HMS), and its occurrence depends on the global moment-shear ratio (Chung et al. 2001; Tsavdaridis and D'Mello 2012).

The size of the web opening and its location within a high-shear zone may cause a non-ductile failure due to tearing and out-of-plane buckling. Chung et al. stated that both shear failure and the VM may occur simultaneously around the web opening (Chung et al. 2003; Lagaros et al. 2008). High global shear forces and a large critical opening length are required to promote such a ductile mechanism and cap deformation demands on non-ductile elements (Chung et al. 2003; Tsavdaridis and D'Mello 2012; Tabar et al. 2022).

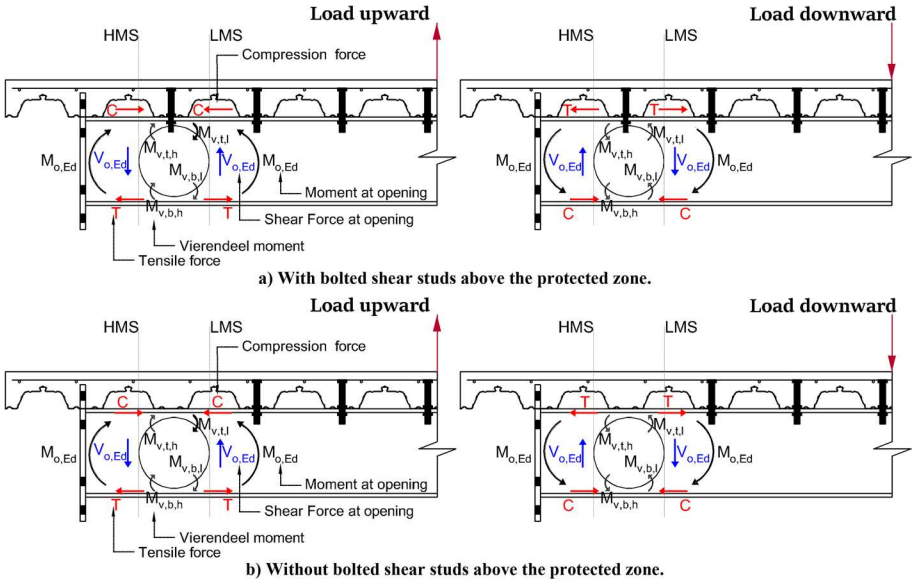

Fig. 2 Forces acting at web opening

Therefore, the failure mode of the perforated section could be controlled by adjusting the web opening location and size critical length for rectangular and elliptically-based web opening shapes is fixed) (Chung et al. 2003; Liu and Chung 2003; Lagaros et al. 2008; Yang et al. 2009; Tsavdaridis and D'Mello 2012; Erfani and Akrami 2017; Tsavdaridis et al. 2017; Shaheen et al. 2018).

Undercyclic loading, the top and bottom Tee-sections will be subjected to global/cross-section shear and moment, as well as local axial forces as shown in Fig. 2. The behaviour of the top and bottom Tee-sections alternates between tension and compression due to the reversible actions expected during earthquakes. Any increase in the global moment will generate local axial forces in the Tee-sections, and decrease their contribution to the capacity of the VM (Lawson and Hicks 2011). An increase in the shear force and critical length will lead to larger moments within the Vierendeel Mechanism.

When the applied load goes upward, moments within the VM cause the web of the top Tee-section to undergo tension while the flange-web of the top Tee-section exhibits compression at HMS (Fig. 3). Under the same conditions, the web of the top Tee-section will

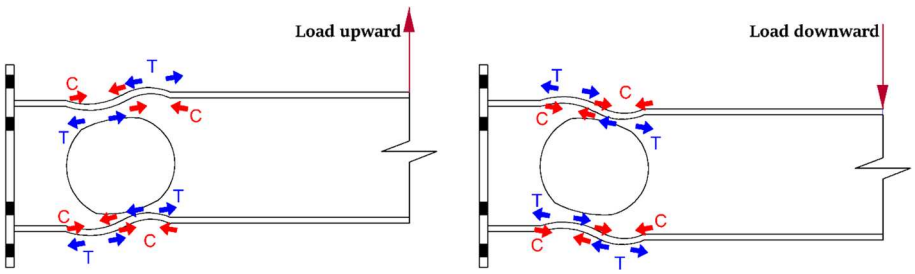

Fig. 3 Axial forces at opening

experience compression while the flange-web and the top Tee-section will be under tension at LMS. Such a complex behaviour can induce early local yielding of Tees before any yielding in the connection and column. This early local yielding results in the stretching of the opening and local buckling of flanges as shown in Fig. 3. Both are indicators of the formation of the Vierendeel (ductile), Mechanism which becomes the dominant mechanism rather than simple vertical shear failure at the web opening, due to the redistribution of the global actions.

3 Experimental program

3.1 Design and details of the composite connection specimens

The initiative involved cyclic load testing on full-scale specimens of four identical steel–concrete composite connections in terms of sizes and material (Table 1 and Fig. 4). Summary of specimen characteristics and material nominal capacities are provided in

Table 1 Specimen test matrix

Specimen ID		Solid Specimen	RWS-L-retrofit*	RWS-L	RWS-H
Connection type		EEP	EEP RWS		
Composite action		Low (L)			High (H)
Web opening	Diameter h_o	–	0.8 h	0.8 h	0.8 h
	End-distance S_o		1 h	0.8 h	0.8 h
Width for end-post S_e (mm)		600			300
$M_{j,Rd}$(kNm)		300.2			
$M_{pl,a,Rd}$ or $M_{o,a,Rd}$ (kNm)		300.2	257.1		
$M_{j,Rd}/M_{pl,a,Rd}$ or $M_{j,Rd}/M_{o,a,Rd}$		1	1.17		
Joint Category		Partial strength	Full strength		
Primary and secondary beams		305 × 165 UB 54			
Column		305 × 305 UC 198			
Bolts		M27 Gr. 10.9 with preloading force of 321 kN			
Slab		140 mm			
Metal deck		ComFlor 60			
Two rows of bolted shear connector		M20 × 160 mm—Gr. 8.8 with preloading force of 40 kN			
# of lines of bolted shear connectors		6			7

*A web opening was created into the solid specimen and then retested for rehabilitation purposes. EEP = extended end-plate. Low (L) = low composite action where the studs are avoided over the protected zone. High (H) = high composite action where the studs are placed over the protected zone. h = height of the beam; 80d = means the diameter of the web opening is equal 80% of h; 80S = means the end-distance is equal 80% of h. $M_{j,Rd}$ = joint capacity. $M_{pl,a,Rd}$= the nominal plastic bending capacity for the steel beam section without a web opening = $F_y W_{pl,y}$ (Eq. 1) according to EC3 (CEN 2005b). $M_{o,a,Rd}$= the nominal plastic bending capacity for the steel section with a web opening = $F_y\left(W_{pl,y} - {d_o}^2.t_w/4\right)$ (Eq. 2) according to SCI-P355 (Lawson and Hicks 2011) and SCI-P428 (Girão Coelho et al. 2020)

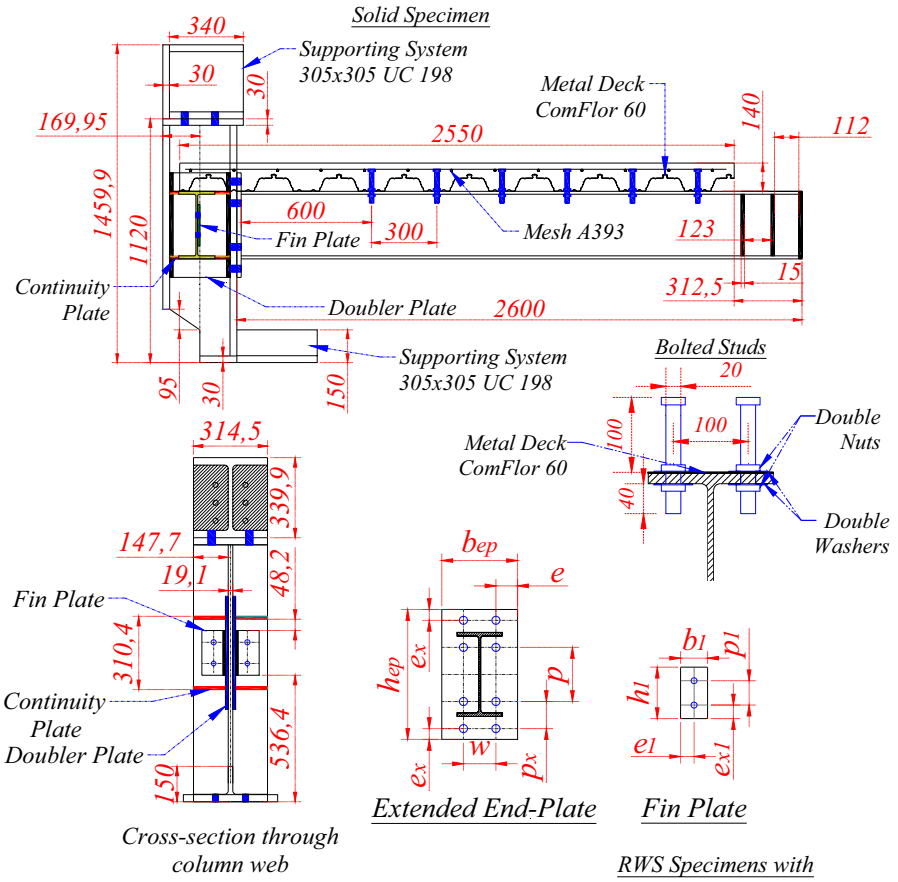

Extended end-plate		Fin plate	
M27 Gr. 10.9		M20 Gr. 10.9	
t_{ep}	20	t_1	10
b_{ep}	280	b_1	100
h_{ep}	480	h_1	190
w	120	e_{x1}	50
e_x	100	e_1	50
p_x	40	p_1	90
e	80	Doubler Plate	480x246.7x12
p	200	Continuity Plate	277.1x135.7x12
Note: all dimensions in mm			

Fig. 4 Dimensions of test specimens (mm)

Tables 1 and 2 . All specimens represented an exterior unstiffened extended end-plate connection in an MRF.

The specimens were designed based on the nominal plastic bending capacity $M_{pl,a,Rd}$, of the connected steel solid-webbed beam of a partial-strength connection without considering the composite action contribution in accordance with EC3, EC4

Table 2 Nominal capacities

Specimen	Steel section/ composite section	Moment resistance (kNm)	
		+ ve (upward)	− ve (downward)
Solid specimen	$M_{pl,a,Rd}$	300.3	300.3
	$M_{pl,Rd}$	491.1	300
RWS-L-retrofit	$M_{o,a,Rd}$	265.3	257.1
	$M_{o,Rd}$	265.3	257.1
RWS-L	$M_{o,a,Rd}$	265.3	257.1
	$M_{o,Rd}$	265.3	257.1
RWS-H	$M_{o,a,Rd}$	265.3	257.1
	$M_{o,Rd}$	272.4	257.1

$M_{pl,Rd}$ = plastic moment resistance of composite unperforated beam, respectively, according to EC4 (CEN 2005d). $M_{o,Rd}$ = plastic moment resistance of composite perforated beam, respectively, according to SCI-P355 (Lawson and Hicks 2011) and SCI-P428 (Girão Coelho et al. 2020)

and EC8 (CEN 2005a, b, c, d). The incorporation of web opening makes the connection go from partial- to full-strength as the capacity of the connected steel beam is reduced. Steel-concrete composite RWS connections complied with SCI-P355 (Lawson and Hicks 2011) and SCI-P428 (Girão Coelho et al. 2020) in terms of end-distance, diameter and bolted shear studs.

The first composite specimen was a partial-strength extended end-plate connection with a solid-webbed beam (hereinafter referred to as the solid specimen). The solid specimen was subjected to cyclic loading, until it reached close to 70% of its positive/sagging moment capacity, thus simulating the effects of moderate seismicity over time, for rehabilitation purposes. Then, a web opening was created, and the specimen was re-tested. It is worth mentioning that the beam was perforated off-site, so the composite slab was dismantled and new M27 bolts were provided.

The re-tested (second) specimen is referred to as the RWS-L-retrofit specimen which was the second specimen to be tested. This allows for benchmarking the effects of residual strains and stresses induced by previous earthquake events. The other two specimens were steel–concrete composite RWS connections. The difference between them is the presence or absence of bolted shear studs above the web opening (i.e., composite action).

The presence/absence of the bolted studs above the web opening was used to classify the specimens as having high (H) or low (L) composite action according to EC8-1 clause 7.7.5 and ANSI/AISC 358–16 (CEN 2005a; ANSI/AISC 358-16 2016) as shown in Table 1. All four specimens had a 25 mm gap between the connection's components and reinforced concrete (RC) slab, to avoid the crushing and cracking of the concrete following ANSI/AISC 358-16 and EC8-1 clause 7.7.5(2) (CEN 2005a; ANSI/AISC 358-16 2016).

A cantilever testing setup was selected to benchmark behaviour. This was accomplished by providing a strong stocky column in such a way that its deformation is negligible. The highly ductile beam section was chosen based on the width-to-depth and span-to-depth ratios according to seismic provisions ANSI/AISC 341-16 and 358-16

(ANSI/AISC 341-16 2016; ANSI/AISC 358-16 2016) and in such way that was feasible to test them the available facilities.

3.2 Materials and Specimen preparation

Steel material of grade S355 was selected, and its properties were validated through coupon tests (Fig. 5). Likewise, the average values of the three compression cylinder tests of RWS-L and RWS-H specimens were 31.28 MPa and 28.72 MPa, respectively. Bolted studs were used (Fig. 4) with a hole clearance of 1 mm to minimise slippage according to SCI-P428 (Girão Coelho et al. 2020). The preloading force of bolted studs was set at 40 kN, which is within the elastic range, thereby allowing for reuse in subsequent cycles.

3.3 Test setup

The test setup consisted of a full-scale one-sided composite extended end-plate RWS connection (see Figs. 6 and 7). The general instrumentation layout for the test setup cyclic and the loading protocol are presented in Figs. 8 and 9. The latter follows the widely accepted AISC 341(ANSI/AISC 341-16 2016). The test setup was designed to minimise deformation contributions from the column. Thus, the back, top and bottom of the strong column were fixed within the testing rig frame. Loading plates were used to connect the specimens to the actuator due to the height limitation of the testing rig frame. Lateral restraints were provided at the point of the actuator connection, to set boundary conditions that resemble what is generally expected in buildings.

4 Experimental results

4.1 Solid connection (no web opening)

The solid connection specimen followed the loading protocol until reaching an imposed chord rotation of 0.02 rad in both directions. At these points, the solid specimen reached 70% and 80% of its positive and negative moment capacities, respectively (Fig. 10 and Table 3). The stiffness degradations in both directions were less than 20%. No signs of plastic deformation were observed, either through visual inspection, or measurements by

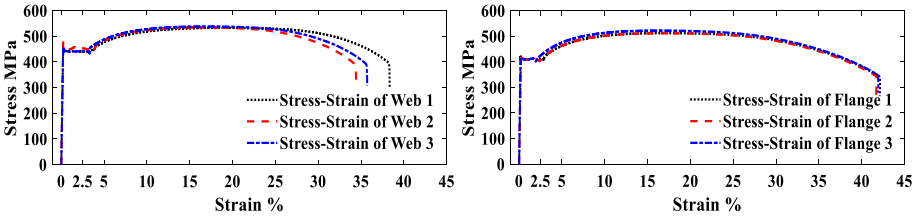

Fig. 5 Coupon Tests for Steel

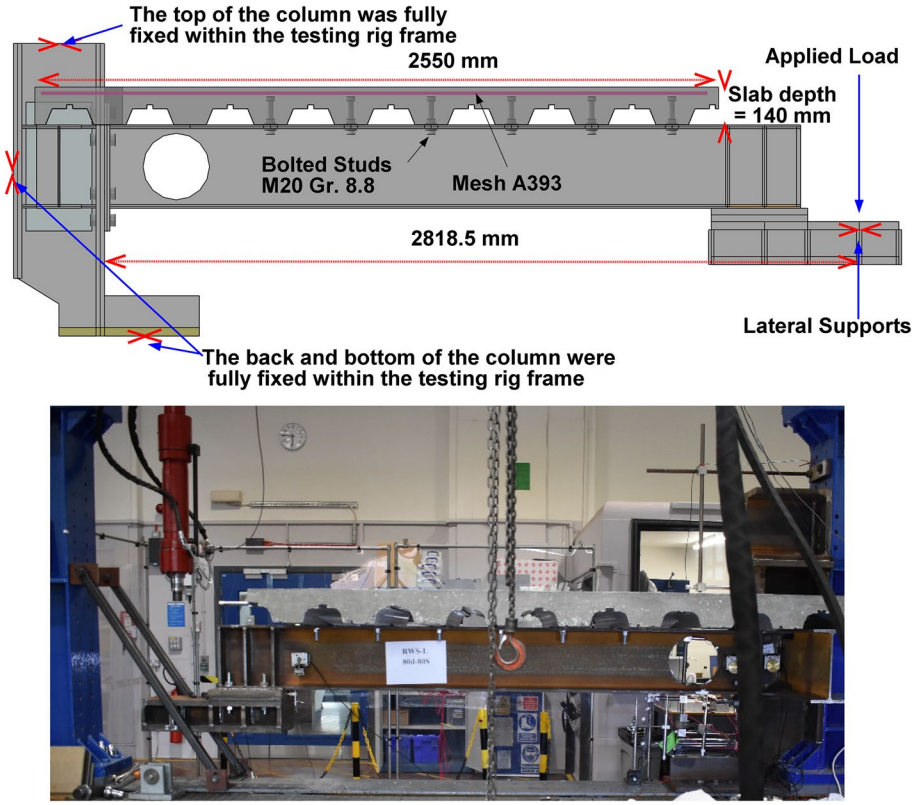

Fig. 6 Experimental test setup—side view

Fig. 7 Experimental test setup—front and top view (mm)

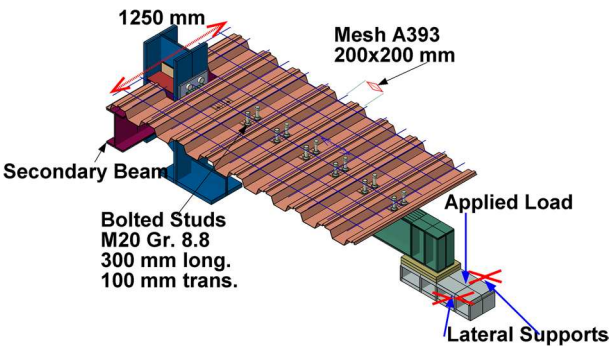

strain gauges. This is a likely outcome of the slab's contribution to increasing the strength of the connection for hogging moments. At most two lines of micro-cracks within the concrete slab were recorded, as shown in Fig. 11. Clearly, the onset of yielding in the solid specimen was reached without extensive plastic actions as illustrated in Fig. 12. All the

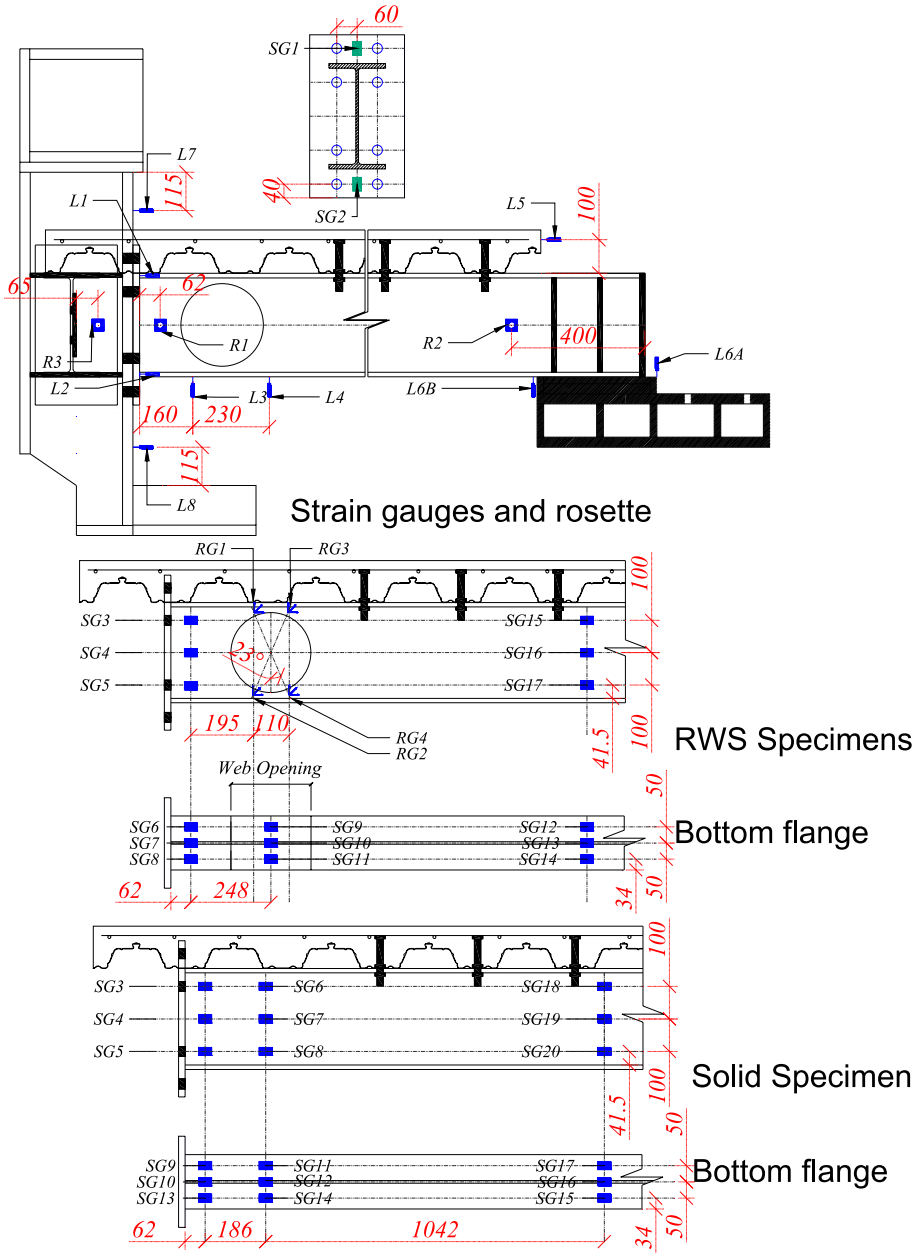

Fig. 8 Instrumentation layout (mm)

other steel elements including the demountable bolted shear studs were damage-free. Consequently, the composite slab was disconnected from the beam to create a web opening to simulate a retrofit procedure. Hence, this leads to the RWS-L-retrofit specimen, as shown in Fig. 13.

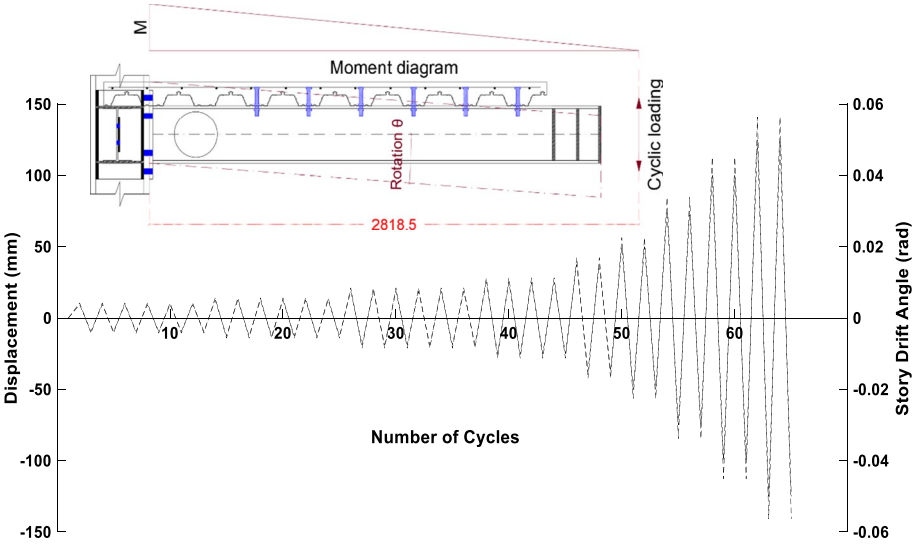

Fig. 9 Cyclic loading protocol

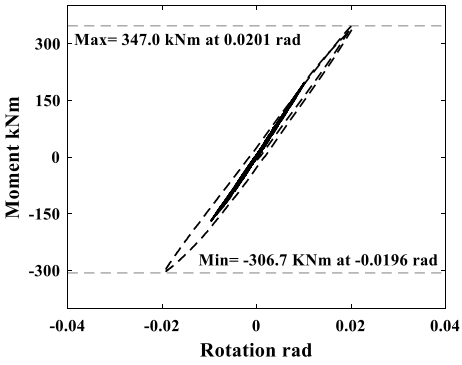

Fig. 10 Moment-Rotation Curve Solid Connection Specimen

4.2 Yielding mode

The development of yielding and plastic hinges in all three RWS connections is presented in Figs. 14, 15, and 16. It is worth reiterating that in this study, LMS and HMS depend on the global applied moment, for instance, the edge of a web opening subjected to lower global moment is LMS (see Fig. 2). Additionally, each side consists of bottom and top Tee-sections.

Recorded strains in the vicinity of the web opening in all RWS connections are larger in the LMS than in the HMS. In RWS-H only, the strain demand at LMS was significantly higher than that at HMS. This was attributed to the composite beam-slab engagement as the shear transfer bolts were placed off-centre over the LMS of the web opening thereby increasing the strain demand on the Tee-sections of the LMS. Consequently, yielding initiated earlier in RWS-H at the bottom Tee-section of the LMS than the other RWS connections during the first cycles of 0.01rad (sagging) as illustrated in Fig. 12. However, the web opening exhibited extensive load redistribution from LMS to HMS in all RWS

Table 3 Results summary

		Solid	RWS-L-retrofit	RWS-L	RWS-H
M at column face M_f (kNm)	+ ve	347	340.2	339.4	328.7
	− ve	− 306.7	− 318.5	− 293.4	− 290.3
M at opening centreline M_o (kNm)	+ ve	–	300.3	307.1	290.1
	− ve	–	− 281.2	− 265.4	− 256.2
$M_f/M_{pl,a,Rd}$ steel section	+ ve	1.16	1.13	1.13	1.09
	− ve	− 1.02	− 1.06	− 0.98	− 0.97
$M_f/M_{pl,Rd}$ composite section	+ ve	0.71	0.69	0.69	0.67
	− ve	− ve $M_f/M_{pl,Rd}$ steel section			
$M_o/M_{o,a,Rd}$ steel section	+ ve	–	1.17	1.19	1.13
	− ve	–	− 1.09	− 1.03	− 1.00
$M_o/M_{o,Rd}$ composite section	+ ve	–	1.13	1.16	1.06
	− ve	− ve $M_o/M_{o,a,Rd}$ steel section			
θ_u(rad)	+ ve	–	0.0499	0.0499	0.0499
	− ve	–	− 0.0499	− 0.0498	− 0.0499
θ_y(rad)	+ ve	0.0201	0.0180	0.0174	0.0168
	− ve	− 0.0196	− 0.0169	− 0.0150	− 0.0148
M_y(kNm)	+ ve	–	323.9	324.1	318.2
	− ve	–	− 294	− 279.5	− 185.2
Ductility $D_\theta = \theta_u/\theta_y$	+ ve	–	2.39	2.91	2.82
	− ve	–	− 2.39	− 3.46	− 3.14
Dissipated energy (kN.m.rad)	+ ve	–	35.20	34.87	34.42

M_f is the applied moment at the column face. M_o is the applied moment at web opening centreline

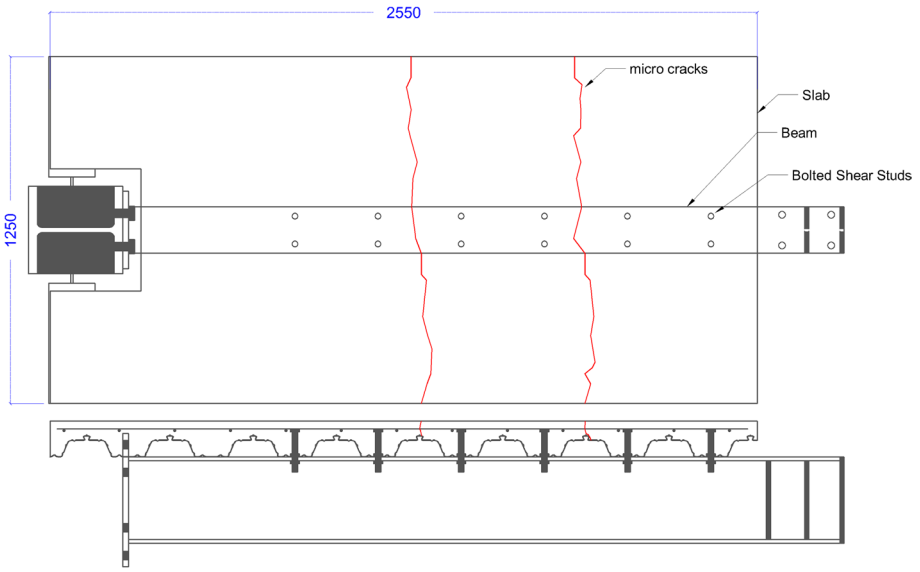

Fig. 11 Observed crack pattern in Solid connection specimen (mm)

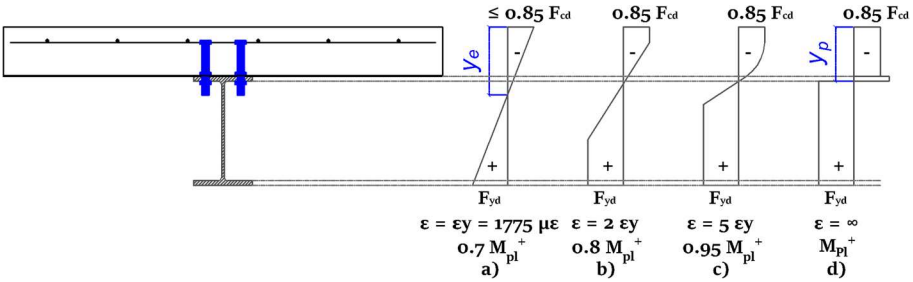

Fig. 12 Elastic, elastic–plastic and plastic stress distributions in a composite section (Davison and Owens 2012)

Fig. 13 Disconnecting the composite slab of the solid connection specimen to be reused for the next test

connections. This can be observed where the Tee-sections of the HMS in all three RWS connections reached yielding before the first two cycles of 0.02 rad.

The web opening experienced large deformation in all three RWS connections when subjected to 0.03rad rotation cycles. The first plastic hinges formed in all three RWS connections at the top tee section of LMS. Particularly, in RWS-H, (see Fig. 17a) there were peeling and hairline cracks starting at the edges of the web opening on the top Tee-section at the LMS.

In all RWS connections, during the first cycle of 0.03 rad, the beam top and bottom flanges (above and below the web openings) began to buckle locally when in compression and straighten out when in tension. This behaviour persisted until the 0.04 rad rotation cycles. This indicates that four plastic hinges around the web opening occurred (Vierendeel Mechanism). Hence, the VM was fully developed, allowing for local buckling of the beam in both its top and bottom flanges. It could be concluded that the local yielding of Tees (ductile failure) led to a favourable behaviour instead of a simple shear failure at the web opening, in all RWS specimens.

4.3 Hysteretic response

The hysteresis curves for all RWS connections are presented in Figs. 18, 19, and 20. Provision of stable hysteresis cycles with a high energy dissipation capacity at well-defined plastic hinge locations, is fundamental for resilient structural behaviour during and in the aftermath of earthquakes (Bernuzzi et al. 1996). In the present study, RWS connections behaved as expected in terms of attaining ductility, mitigating the cracks of concrete slabs,

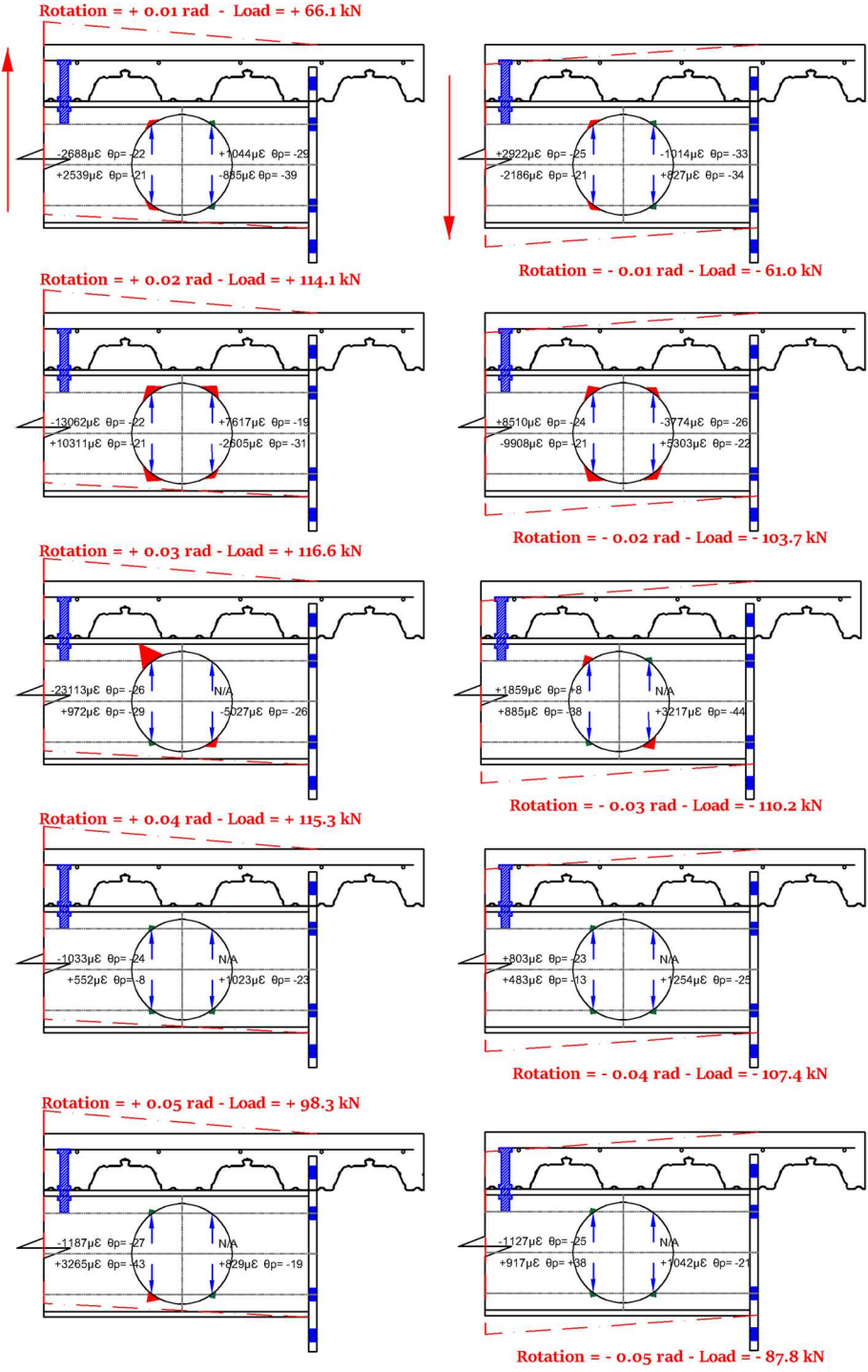

Fig. 14 Distribution of strain intensity for RWS-L-retrofit connection (N.A. = Not Available due to the lose of the strain gauge during the test)

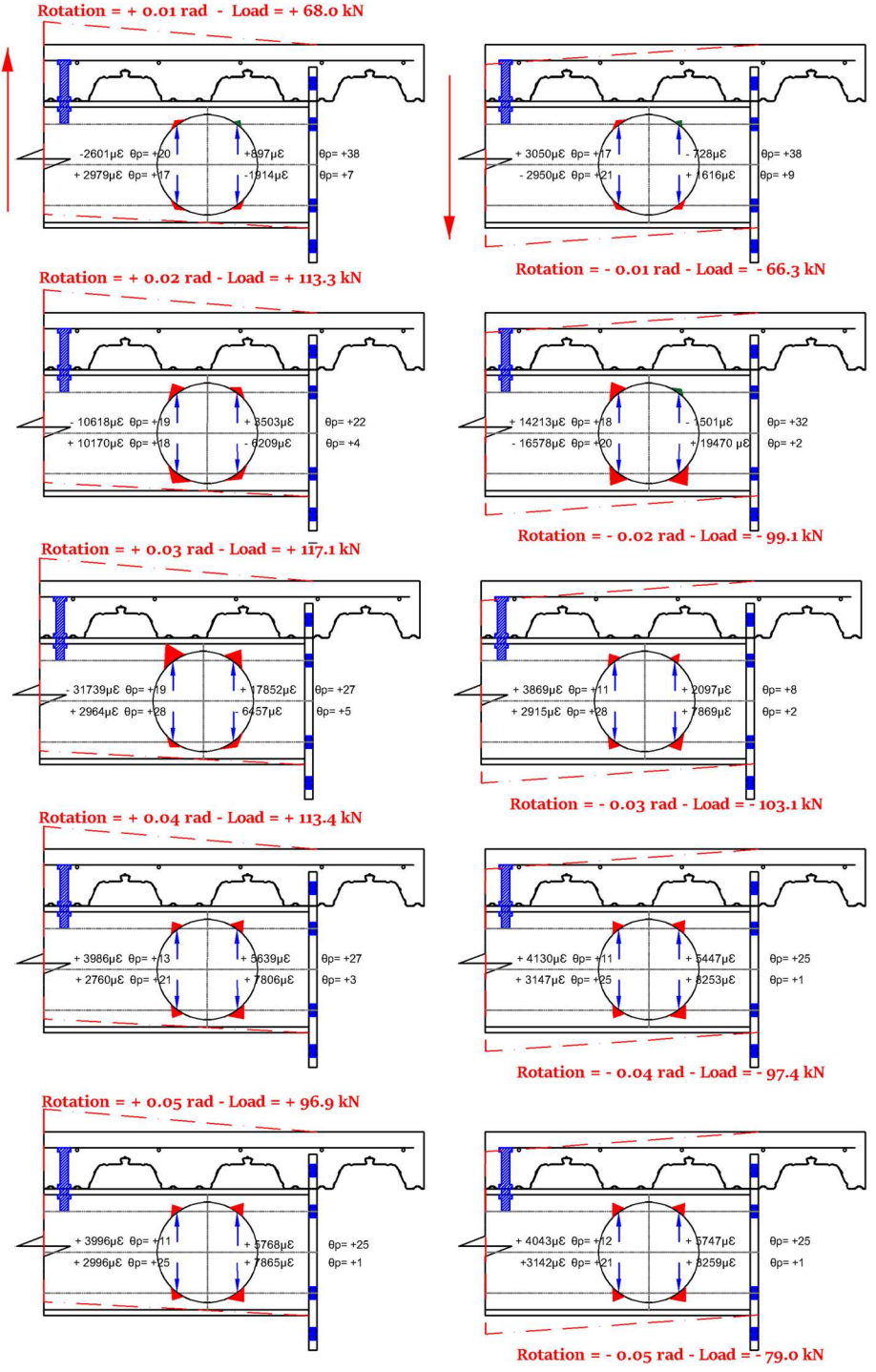

Fig. 15 Distribution of strain intensity for RWS-L connection

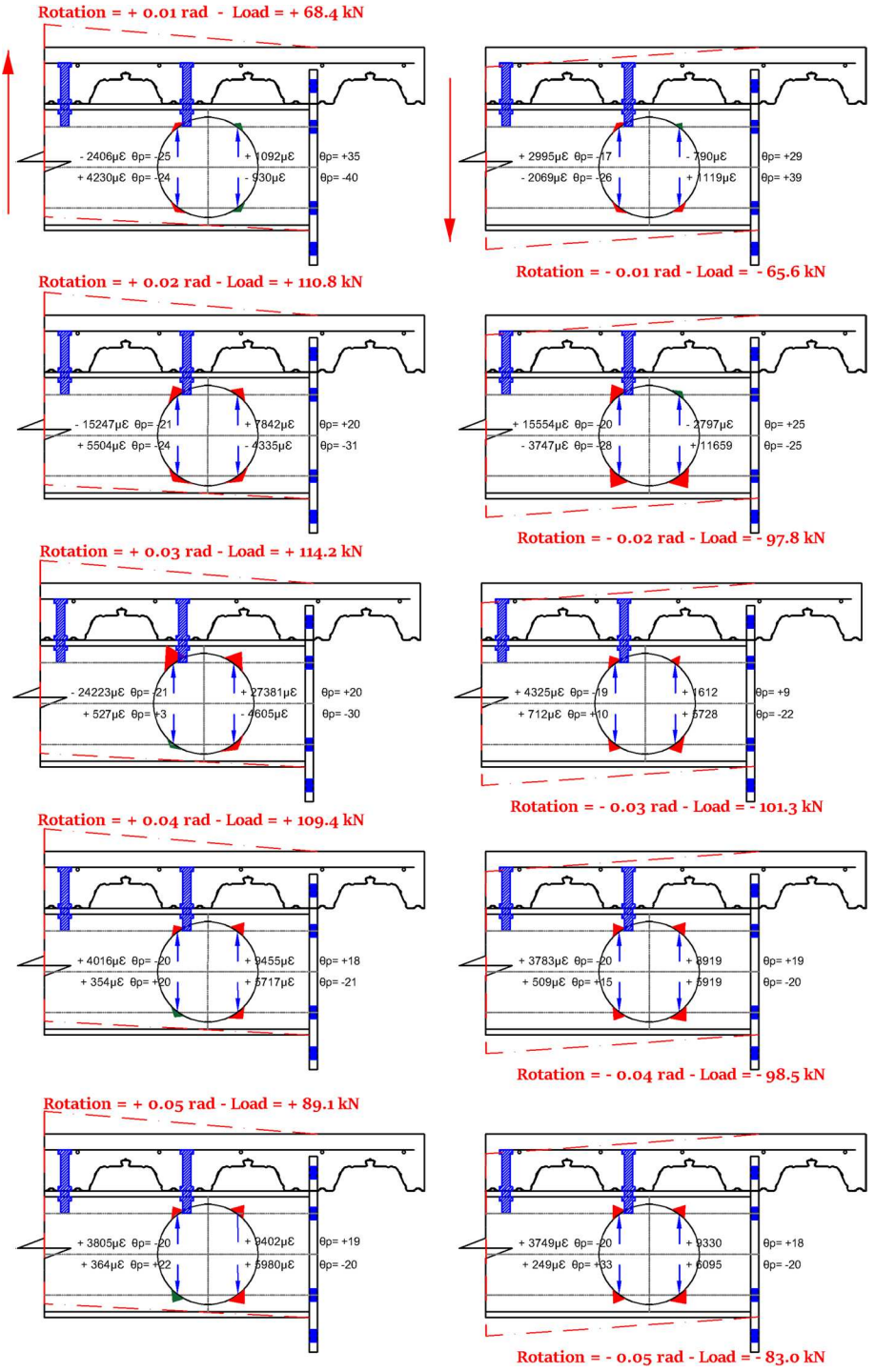

Fig. 16 Distribution of strain intensity for RWS-H connection

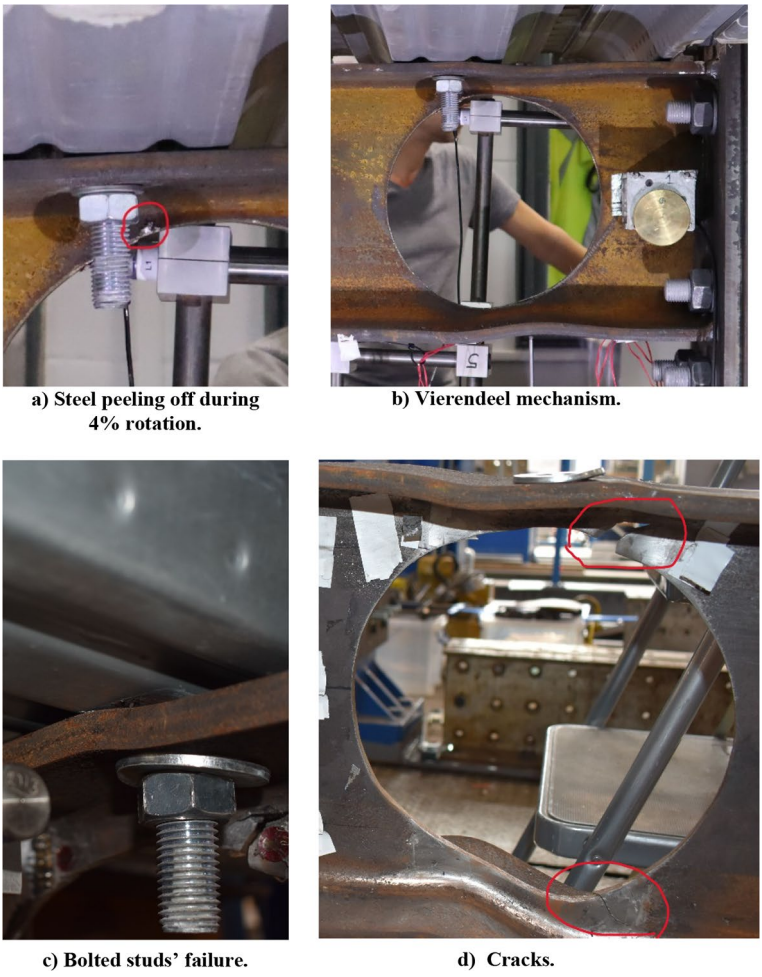

Fig. 17 The failure modes of RWS-H connection

and sustaining higher moments than the bare steel beam's full plastic moment (M_{pl}) at 4% rotation in both directions. Thus, all RWS connections were capable of achieving at least an interstory drift larger than 4%, thereby complying with performance targets set up in of ANSI/AISC 358-16, ANSI/AISC 341-16 and the EC8 (CEN 2005a; ANSI/AISC 341-16 2016; ANSI/AISC 358-16 2016). It must be stressed that rotation capacity is expected to be larger when deployed in moment-resisting frames due to column flexibility.

Round hysteresis cycles without pinching were observed for all RWS connections. They are the outcome of early local yielding in the vicinity of the web opening, thus, leading to the redistribution of the global actions from LMS to HMS. This redistribution is due to inelastic stresses being concentrated around the web openings, inducing the occurrence of the VM in the weakened area of the beam rather than failure within its non-ductile components. Such a mechanism caps the shear forces that can be transferred outside the protected zones, in close alignment with capacity design principles.

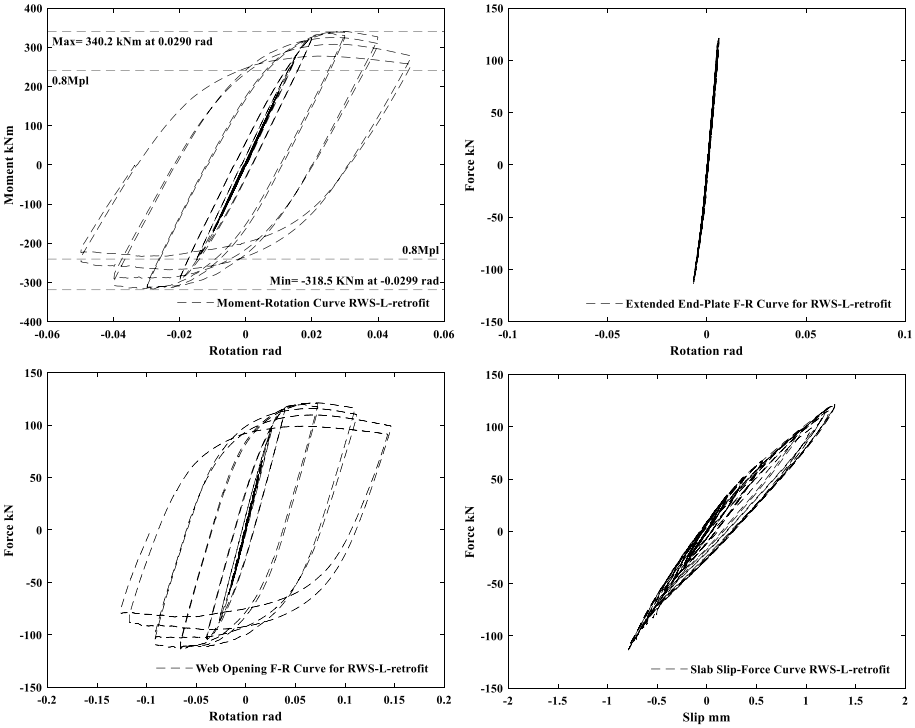

Fig. 18 Hysteretic curves for RWS-L-retrofit connection

It was expected that the extra row of studs over the protected zone would lead to early yielding and early failure due to increased stress/strain demand on the bottom flange (Lee et al. 2016). However, energy dissipated well through the VM in RWS-H, despite earlier crack initiation in the vicinity of the web opening. This was attributed to the capability of the web opening for redistribution of local forces, counterbalancing the increased stress/strain demand on the bottom flange that led to quick initiation of a crack in the vicinity of the web opening.

Unexpectedly, RWS-H demonstrated lower moment capacity compared to the identical specimen RWS-L (Table 3). The extra row of bolted shear studs should have led to a higher moment capacity of the RWS-H specimens when compared with their counterparts. Instead, it increased the stress/strain demand in the top Tee-section (Fig. 21), leading to an earlier onset of yielding in the top Tee-section at LMS due to the location of the extra row of bolts above the LMS. This can be justified by the fact that the web opening consists of two Tee-sections (top and bottom sections) with similar local behaviour under the same global load. Each Tee-section consists of top and bottom parts that exhibit compression and tension under the same action over the cross-section, as illustrated in Fig. 21. The location of the studs above LMS led the bottom part of the top Tee-section to experience earlier local yielding, which eventually induced earlier crack initiation at the LMS as well. This is a plausible explanation for the lower moment capacity of RWS-H, as this feature was absent in RWS connections without composite action above the web opening.

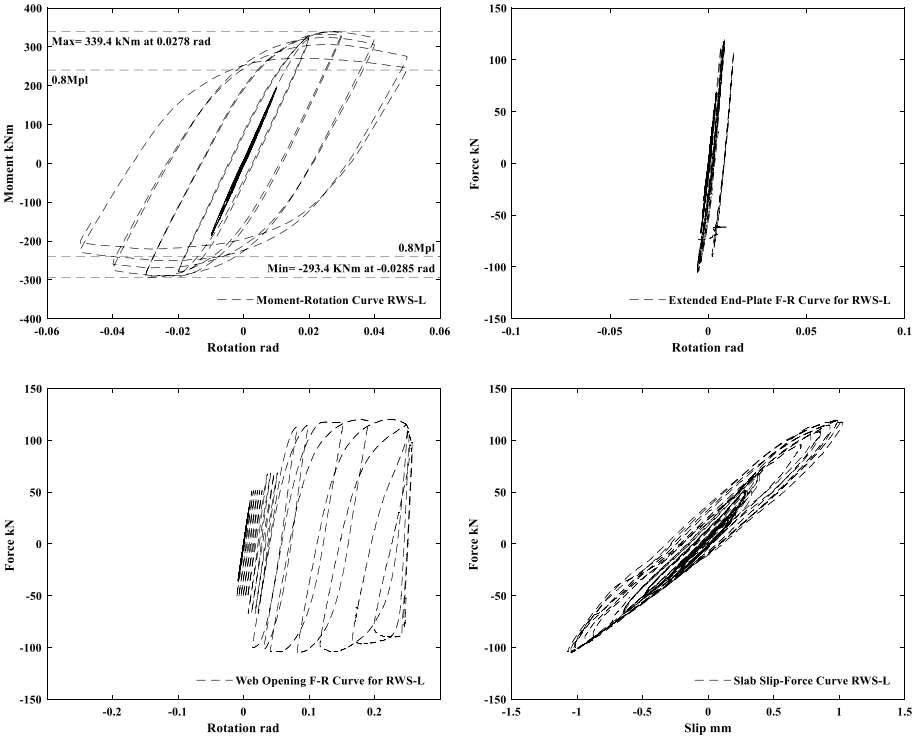

Fig. 19 Hysteretic curves for RWS-L connection

Remarkably, the retrofitted specimen (RWS-L-retrofit), which involved creating a web opening, performed as well as the other RWS connections, despite concrete cone failure (Fig. 22b.). Another crack line was observed in the slab of RWS-L-retrofit connection (Fig. 23), in addition to the two lines of micro-cracks that developed in the solid connection as illustrated in Fig. 11. These two lines of cracks became more visible but did not propagate deeply inside the slab in the next test of RWS-L-retrofit. While RWS-L and RWS-H specimens experienced only micro-cracks. Also, slight separation between the metal deck and the concrete occurred in RWS-L and RWS-L-retrofit (see Fig. 24). The maximum slab slip in all RWS connections at the maximum load was not more than 1.3 mm in the positive moment and 1.32 mm in the negative moment. This further indicates that significant plastic deformation only occurred in the web opening.

It seems that both the demountable shear studs and a 25 mm gap between the slab and steel elements played a key role in mitigating concrete slab damage, along with the plastification of the web opening. This could be due to the hole clearance in the steel beam flange which allowed for slippage between the beam and the slab, as well as the fact that plastic deformation occurred in the vicinity of the web opening. The provision of the entirely disconnected beam-to-column joints (i.e., 25 mm gap) prevented contact between the slab and steel elements, thus limiting force transfer between them.

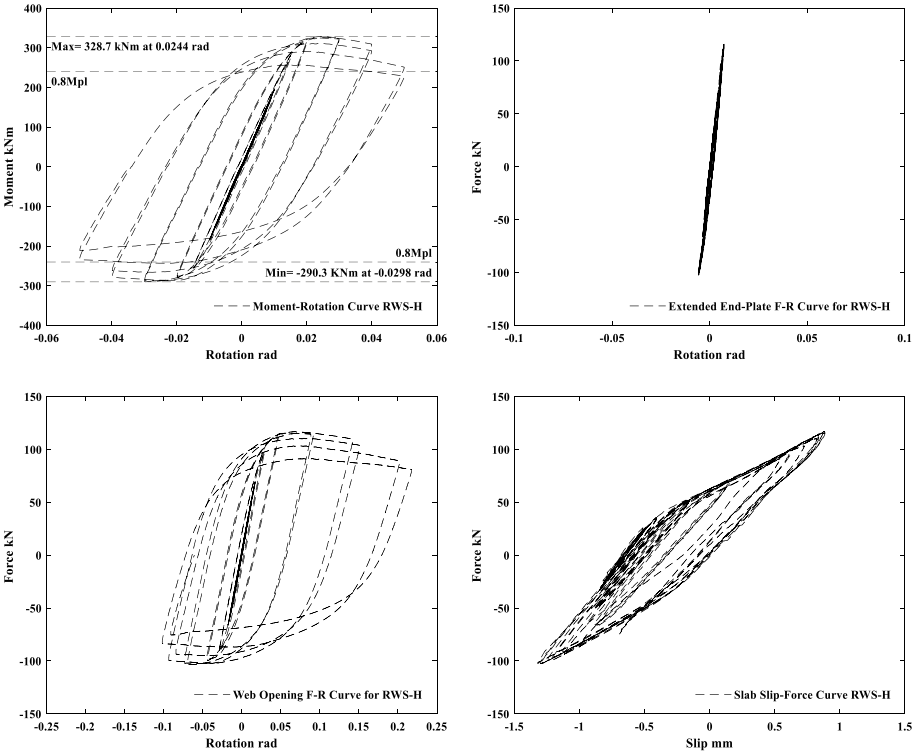

Fig. 20 Hysteretic curves for RWS-H connection

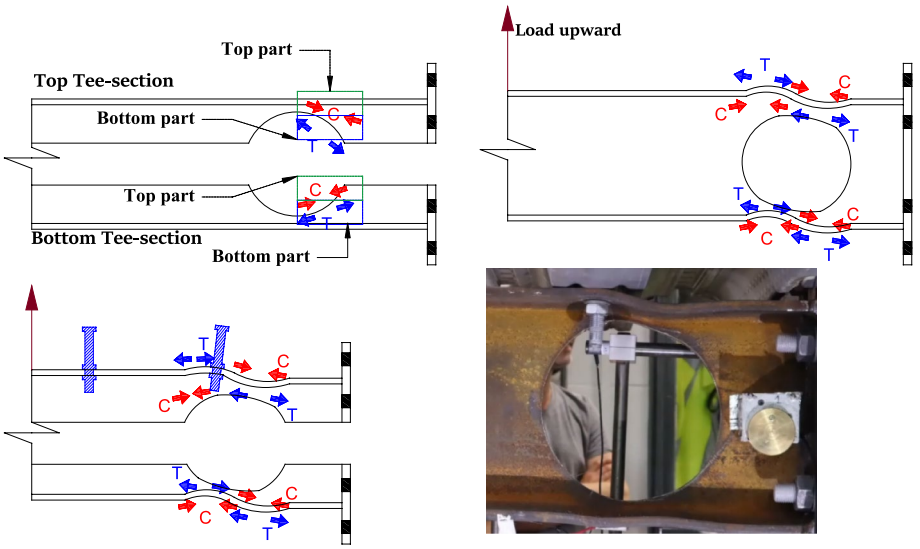

Fig. 21 Illustration of the behaviour of Tee-sections in RWS-H

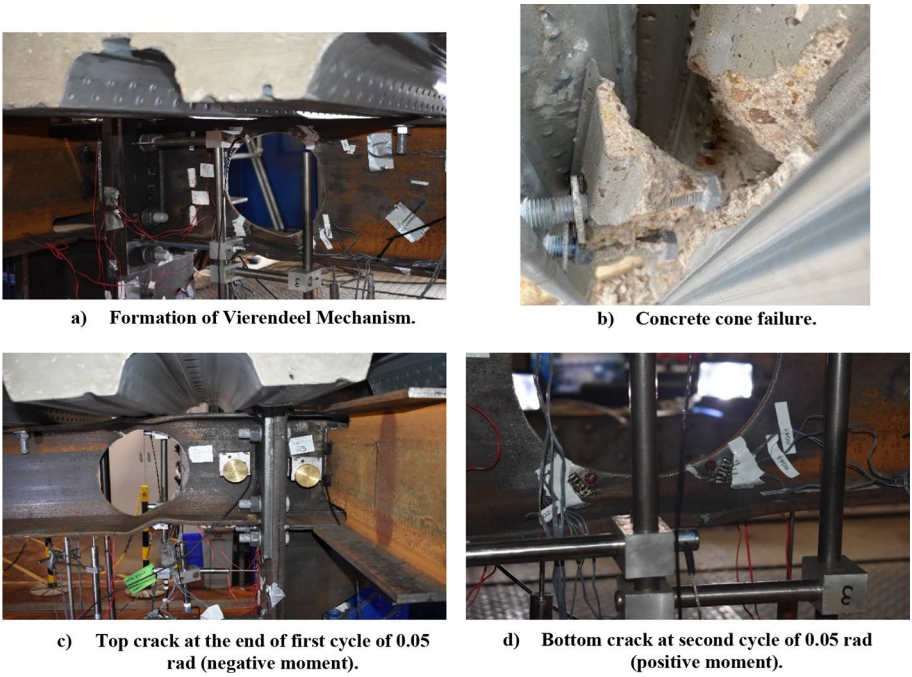

Fig. 22 Failure modes of RWS-L-retrofit specimen

Consequently, the expected failure mode of a ductile frame strong column-weak beam was observed in all tested RWS specimens (Figs. 22 and 24).

The demountable composite system was found to be capable of quick disassembly, therefore fostering reuse, and/or replacement in case of extensive damage observed at the end of the design life or in the aftermath of a large earthquake. The nuts were easily demounted using an ordinary wrench; even, if there was appreciable bending of the washer, which was the case for the RWS-H specimen.

4.4 Expected versus actual resistances

4.4.1 Capacity design

The strong-column weak-beam design framework, adopted in both Eurocodes and AISC (CEN 2005a, c; ANSI/AISC 341-16 2016; ANSI/AISC 358-16 2016) requires that the bending strength of the connection $M_{j,Rd}$ should be stronger than the bending resistance of the connected beam $M_{pl,Rd}$. In this study, the capacity of the connection $M_{j,Rd}$ that was designed based on the components method in EC3-1-8 (CEN 2005c) compared to $M_{pl,a,Rd}$ and $M_{o,a,Rd}$ are shown in Table 1.

The connection to beam capacity ratio $M_{j,Rd}/M_{pl,a,Rd}$ of the solid specimen equals one, which falls into the category of partial strength according to EC3-8 (CEN 2005c). In the equal/partial strength category, the plastic deformations occur in both the connection and the beam (Landolfo 2022). The introduction of the web opening (RWS) into the solid-webbed beam reduced the capacity of the connected beam. Thus, it increased the

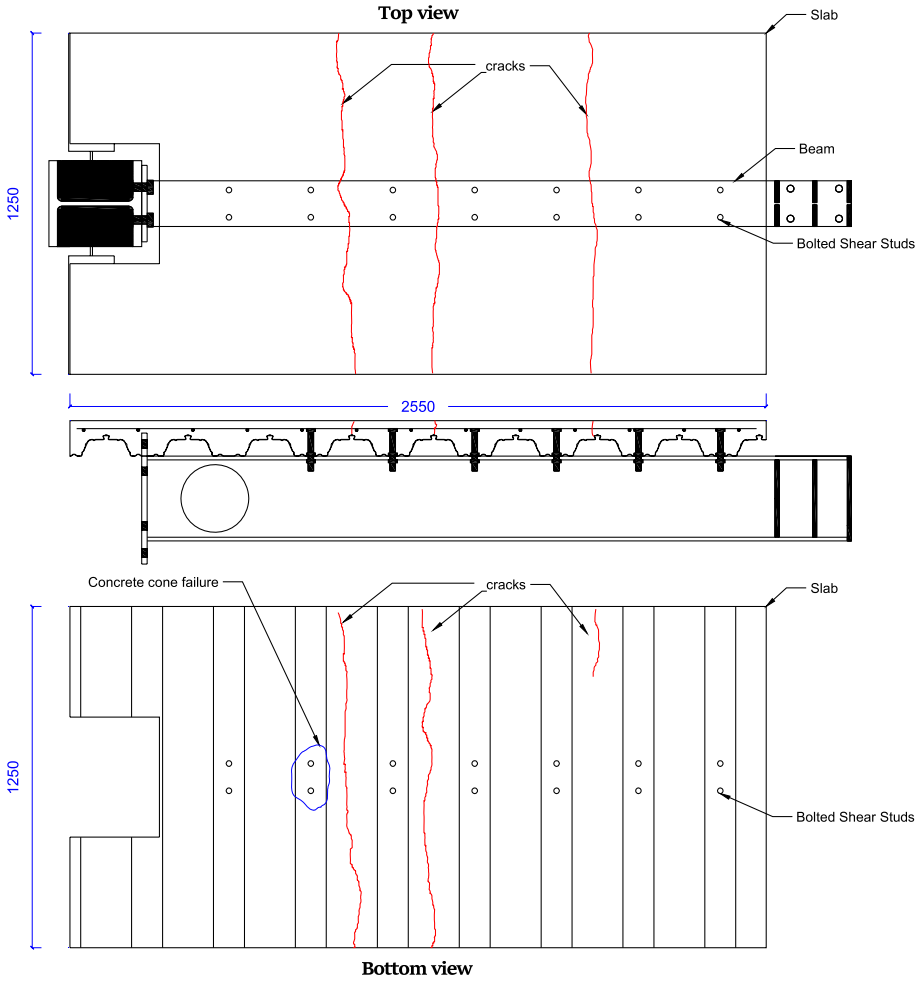

Fig. 23 Observed crack pattern in RWS-L-retrofit connection specimen and concrete cone failure (mm)

connection-to-beam capacity ratio $M_{j,Rd}/M_{o,a,Rd}$ to 1.17 and altered the connection category from partial to full strength.

The adopted capacity design framework was effective for obtaining the expected performance, namely plastic deformations occurred in the web opening only. This means that a web opening effectively constrains inelastic action in the protected zone, away from the joint plate and the column. Henceforth, providing the web opening is a reliable course of action that allows for full-strength connections within the strong column/connection weak beam paradigm.

Ensuring that RWS connections retain their ability to carry gravity forces, even after failure, is critical; especially in the aftermath of an earthquake. In this testing campaign, a large web opening equal to 80% of the beam depth was tested; this exceeds the limitations of the SCI-P355 guidance (Lawson and Hicks 2011). Moreover, as previously mentioned, the rotation capacity is expected to be greater when deployed in

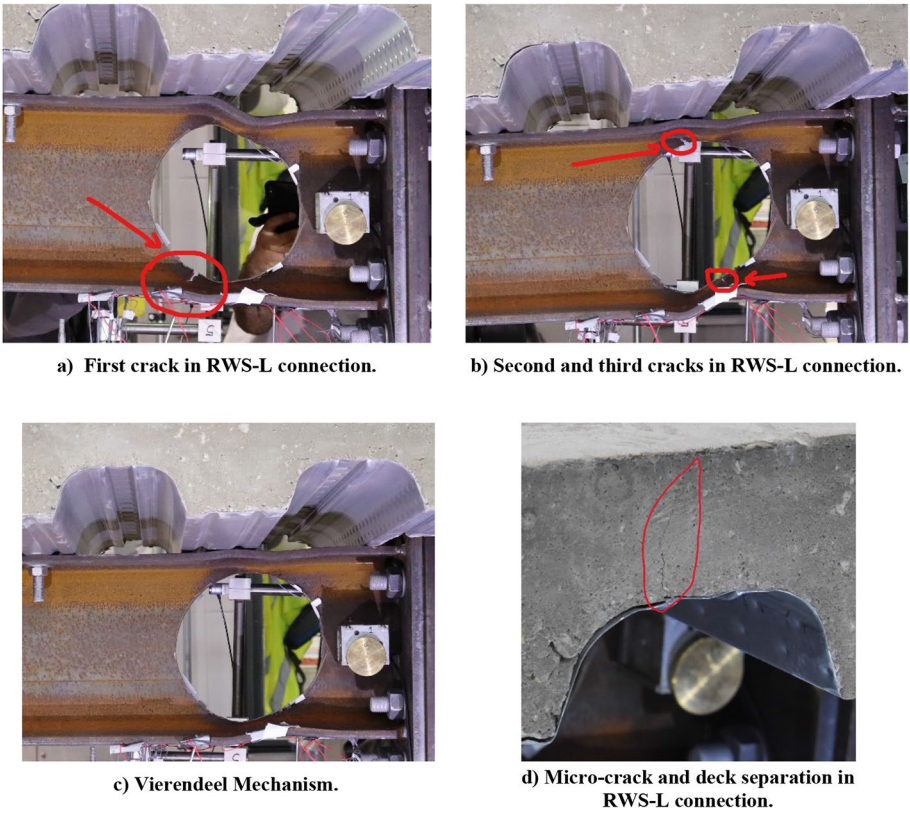

Fig. 24 The failure modes of RWS-L connection

moment-resisting frames than what was observed in these tests, due to the flexibility of the column. As a result, both the column flange and the panel zone would contribute to inter-story drift capacity, preventing cracks in the vicinity of the web opening. Thus, the post-earthquake capacity (e.g., shear capacity) would remain uncompromised, as the Vierendeel capacity of the perforated section would not be reached. The potential risks, such as yielding or buckling of the remaining web sections and their implications for maintaining structural integrity in post-earthquake scenarios, are worth exploring and investigating.

4.5 Connection design moment

Table 3 shows the ratios of the applied actions to the design/capacity values. It is worth noting that all hogging (−ve) design capacities for all non-composite and composite, unperforated and perforated beam sections were based on the steel capacities (i.e., $M_{pl,a,Rd}$ (Eq. 1) and $M_{o,a,Rd}$ (Eq. 2) Table 1). For RWS connections, the average ratios based on the nominal resistance of steel solid-webbed beam (Eq. 1) are + 1.12 and − 1.00 under sagging and hogging moments, respectively. While the average ratios based on perforated steel (Eq. 2), are + 1.16 and − 1.04 under sagging and hogging moments, respectively. Ratio

values greater than 1.00 denote that the composite slab contributes to the overall connection strength.

It is found that under sagging moment, the composite slab contributes to the overall RWS connection strength, regardless of composite engagement. While under hogging moments, the contribution of the composite slab was affected by the location of the web opening. Therefore, the composite action should be considered in the design process due to its contribution. This is because it could jeopardise the strong column-weak beam framework, by strengthening rather than weakening of the beam, if it is not properly accounted for. Further experimental and FE investigations are needed to verify the effect of the size and location of web openings on the contribution of the composite slab.

For sagging moments, it can be seen that the plastic stress block method $M_{pl,Rd}$ overestimates the actual composite section strength (Table 3). While the plastic bending resistance of the composite beam section at the web opening $M_{o,a,Rd}$ according to SCI-P355 (Lawson and Hicks 2011), underestimates the actual composite perforated beam section strength. In details, $M_{o,a,Rd}$ based on the SCI-P355 (Lawson and Hicks 2011), provides an overstrength by about 12%. While the plastic stress block method $M_{pl,Rd}$ does not represent the actual strength and provide less strength than the actual one by about 32%. Hence it is important to comprehend the impact of the composite engagement on RWS connections to consider the overstrength in both new buildings and seismic retrofit.

Regarding moments within the VM, the design method of SCI-P355 (Lawson and Hicks 2011) did not accurately predict the actual Vierendeel bending resistance of the perforated beam section that was subjected to cyclic loading (Table 4). Under sagging moment, the applied Vierendeel moments were lower than the Vierendeel bending resistance by 26% for RWS connection without composite engagement, and by 50% for RWS-H. While under a hogging moment, the applied Vierendeel moments were, on average, 28% lower than

Table 4 Design resistances versus applied actions

RWS connections		RWS-L-retrofit	RWS-L	RWS-H
$V_{o,Rd}$(kN)	Steel	142.9		
	Composite	161.2	160.5	160.5
$M_{V,Rd}$(kNm)	Steel	18.2		
	Composite	18.2		24.5
V_{Ed}(kN)	+ ve	120.7	120.4	116.6
	− ve	− 113	− 104.1	− 103
$M_{V,Ed}$(kNm)	+ ve	13.43	13.40	12.98
	− ve	− 12.58	− 11.59	− 11.46
$V_{Ed}/V_{o,Rd}$	+ ve	0.75	0.75	0.73
	− ve	− 0.79	− 0.73	− 0.72
$M_{V,Ed}/M_{V,Rd}$	+ ve	0.74	0.74	0.53
	− ve	− 0.69	− 0.64	− 0.63

$V_{o,Rd}$ = shear resistance for perforated section and $M_{V,Rd}$ = Vierendeel bending resistance according to SCI-P355 (Lawson and Hicks 2011). V_{Ed} = maximum applied shear force in the test. $M_{V,Ed}$ = applied Vierendeel moment in the test = $V_{Ed}l_e$. Where l_e is equivalent rectangular opening length (Lawson and Hicks 2011). $M_{V,Rd}$ of RWS-L-retrofit and RWS-L for composite sections were based on the steel sections, because there was no composite engagement over the opening (Lawson and Hicks 2011). For − ve $V_{Ed}/V_{o,Rd}$ and − ve $M_{V,Ed}/M_{V,Rd}$, steel section resistances were used (i.e., $M_{V,Rd}$ for steel and $V_{o,Rd}$ for steel)

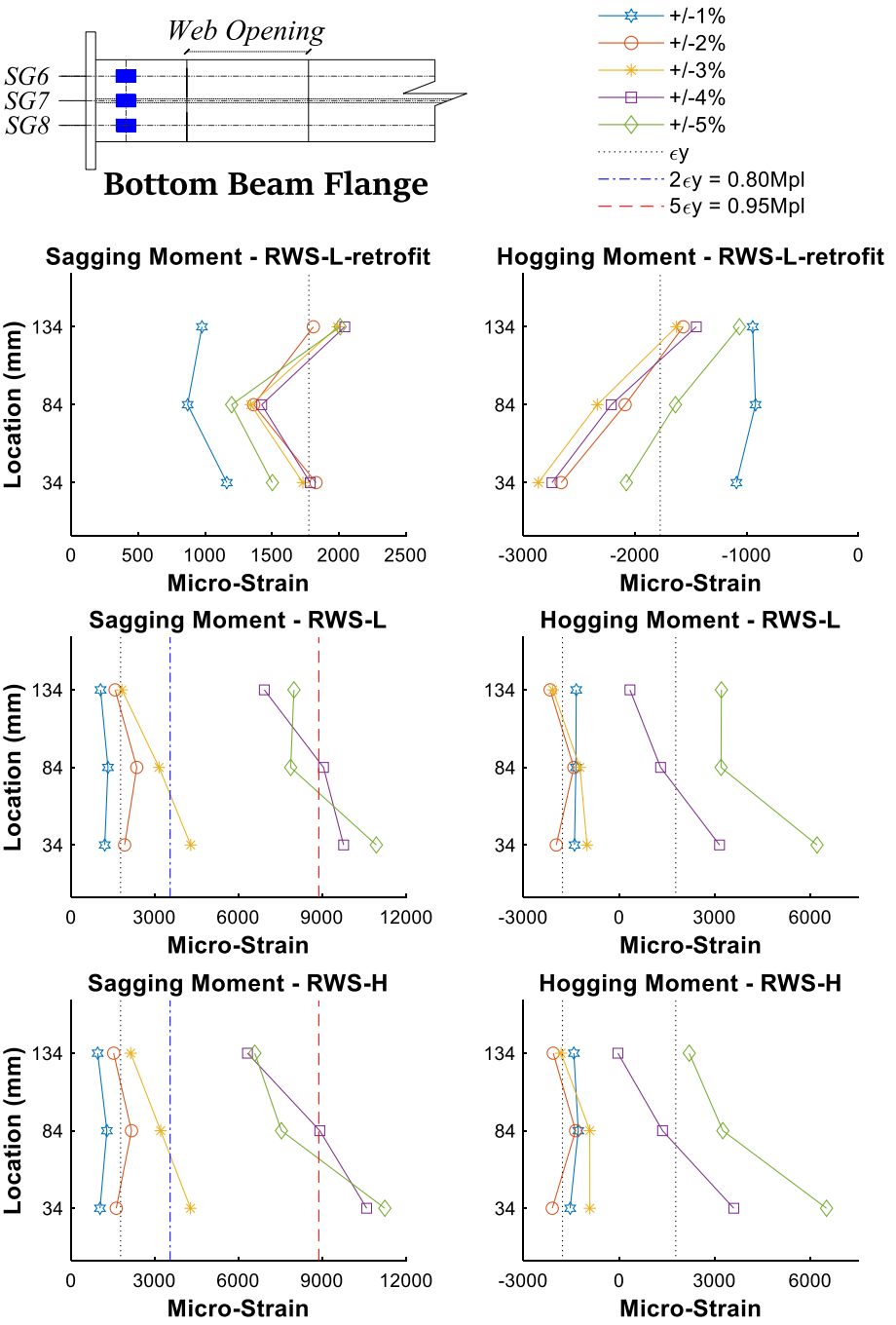

Fig. 25 Strain profiles for beam bottom flange near the connections

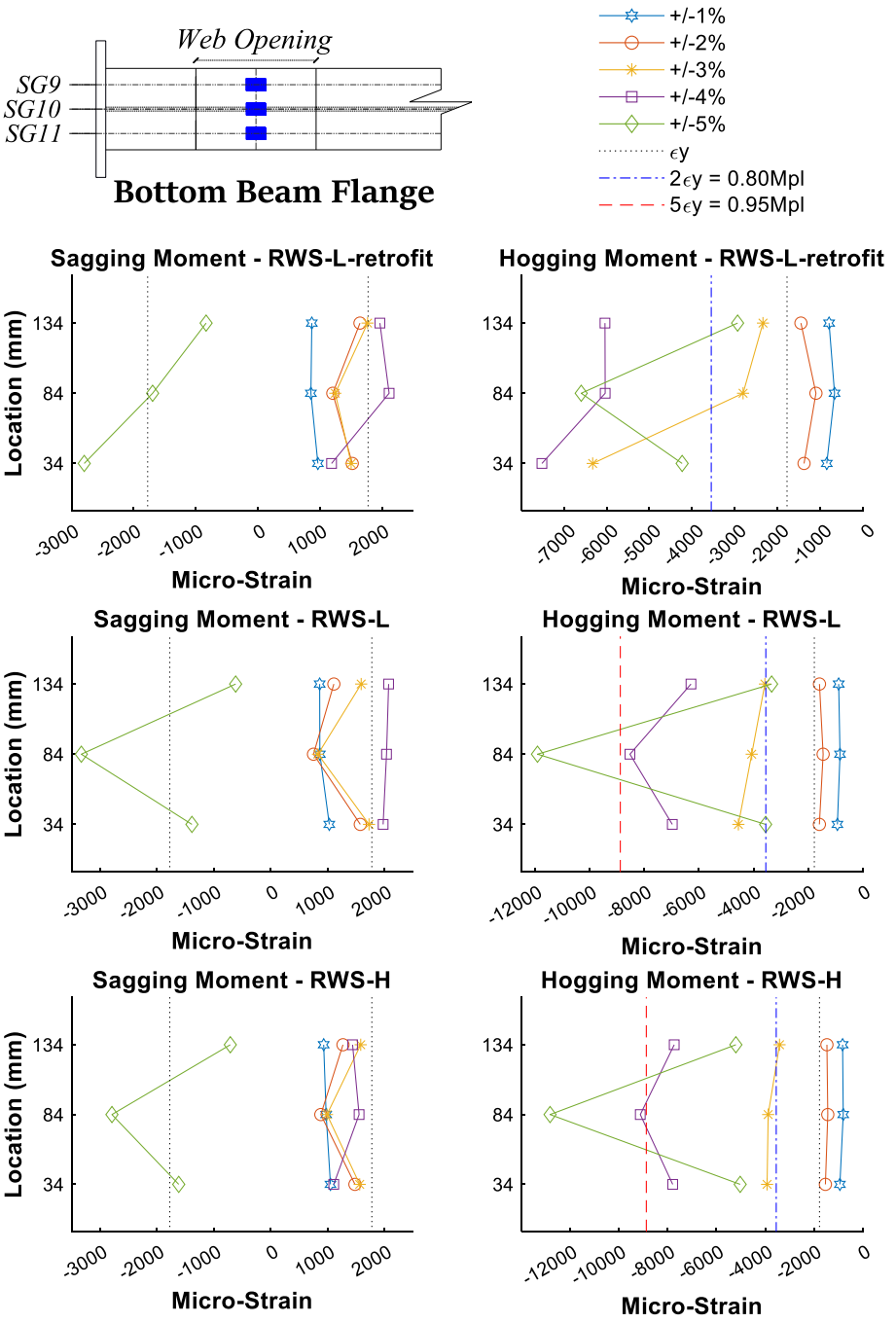

Fig. 26 Strain profiles for beam bottom flange below the web openings

the Vierendeel bending resistance. This also applied to the shear resistance of the perforated sections as per SCI-P355 (Lawson and Hicks 2011). On average, the applied shear forces were 26% and 25% lower than the resistances under sagging and hogging moments, respectively.

4.6 Strain profile across the steel beam bottom flanges

The strain profiles across the steel beam bottom flanges near the connections and below the web openings are presented in Figs. 25 and 26. The strain on the bottom flange near the connection for RWS-L-retrofit was beyond the elastic limit (in yielding region), but did not reach the plastic region as illustrated in Fig. 12. The highest recorded strain was 2866 μ at rotation of 0.03 rad under hogging moments. In contrast, for RWS-L and RWS-H, the highest recorded strains on the bottom flanges near the connection were 10,936 μ and 11,241 μ at a rotation of 0.05 rad under sagging, respectively. The higher strain demands found in RWS-L and RWS-H were approximately 3.8 times those found in the RWS-L-retrofit. This was due to the fact that the location of web openings was closer to the column face in these two connections. This also implies that the strain demand on the bottom flange near the connection was not influenced by the composite engagement, given the negligible difference in the strain demand observed between RWS-L and RWS-H.

Regarding the strain demand on the flange below the web opening, the highest recorded strain was 7516 μ at a rotation of 0.04 rad for RWS-L-retrofit. At the same stage, the recorded strains were 8524 μ and 9122 μ at a rotation of 0.04 rad in RWS-L and RWS-H, respectively. However, the highest recorded strains in RWS-L and RWS-H were 11,907 μ and 12,821 μ at a rotation of 0.05 rad under hogging, respectively. It was observed that under sagging moments, the strain demands on the flange below the web opening did not exceed 3329 μ for all RWS connections. However, the beam flange below the web opening was in the elastic–plastic region during the cycles of 0.03 rad. It was worth noting that the strain profiles up to the end of the tests across the beam web in all RWS connections did not exceed 1603 μ.

5 Conclusions

This paper presents the results of an experimental study of demountable steel-concrete composite reduced web section (RWS) connections to assess their adequacy for use in seismic areas. Four demountable steel-concrete composite connection specimens that employed RWS were tested under cyclic loading. The key differences among the specimens were the presence of bolted shear studs over the web opening and the location of the web opening.

One solid-webbed specimen was tested to examine the structural performance of retrofitted connections. This was done by cutting a hole in the web after subjecting the specimen to cyclic loads representing moderate seismicity. The test results showed that the RWS connections were capable of utilizing the perforation's location in a high shear zone. This resulted in the initiation of local yielding in Tee-sections, leading to the dominance of the ductile (Vierendeel) failure mode in the connected beam.

This mechanism is critical to avoid transferring excessive shear forces to the components of such connections. The results also underscored that the component method

approach used in EC3 for joint design should include the effect of web opening on the joint behaviour using the design guidelines of SCI-P355 (Lawson and Hicks 2011). This is due to the reliability of the occurrence of Vierendeel failure mode.

All specimens are capable of accommodating at least a 4% inter-story drift ratio. This would rank the connections as highly ductile, henceforth allowing for their deployment within Special Moment Resisting Frames (SMRFs), considering both AISC and Eurocode guidelines.

The size and location as well as the presence of bolted studs over the protected zone influence the strength, rotational capacity, ductility, and energy dissipation of RWS connections. Further experimental and numerical studies are required to expand data for potential prequalification in existing and next-generation seismic codes for steel design.

Funding The authors would like to thank SC4 Ltd. for their technical support and providing test consumables.

Declarations

Conflict of interest The authors have not disclosed any competing interests.

Open Access This article is licensed under a Creative Commons Attribution 4.0 International License, which permits use, sharing, adaptation, distribution and reproduction in any medium or format, as long as you give appropriate credit to the original author(s) and the source, provide a link to the Creative Commons licence, and indicate if changes were made. The images or other third party material in this article are included in the article's Creative Commons licence, unless indicated otherwise in a credit line to the material. If material is not included in the article's Creative Commons licence and your intended use is not permitted by statutory regulation or exceeds the permitted use, you will need to obtain permission directly from the copyright holder. To view a copy of this licence, visit http://creativecommons.org/licenses/by/4.0/.

References

Almutairi FF, Tsavdaridis KD, Alonso Rodriguez A, et al (2023) Hysteretic behaviour of composite reduced web section (RWS) connections for seismic applications. J Earthq Eng 1–36

ANSI/AISC 341-16 (2016) Seismic provisions for structural steel buildings. Seism provisions Struct steel Build 60601

ANSI, AISC 358–16 (2016) Prequalified connections for special and intermediate steel moment frames for seismic applications. AISC, IL

Ataei A, Bradford MA, Valipour HR, Liu X (2016) Experimental study of sustainable high strength steel flush end plate beam-to-column composite joints with deconstructable bolted shear connectors. Eng Struct 123:124–140

Ataei A, Bradford MA, Liu X (2017) Computational modelling of the moment-rotation relationship for deconstructable flush end plate beam-to-column composite joints. J Constr Steel Res 129:75–92

Ataei A, Zeynalian M, Yazdi Y (2019) Cyclic behaviour of bolted shear connectors in steel-concrete composite beams. Eng Struct 198:109455

Bernuzzi C, Zandonini R, Zanon P (1996) Experimental analysis and modelling of semi-rigid steel joints under cyclic reversal loading. J Constr Steel Res 38:95–123

Bi R, Jia L, Li P, Wang Q (2021) Multiparameter seismic behavior of castellated beam-to-column connections based on stress migration. Structures. Elsevier, Amsterdam, pp 1137–1153

CEN (2005a) Eurocode 8: Design of structures for earthquake resistance-Part 1: General rules, seismic actions and rules for buildings. Eur Commun Stand Bruss

CEN (2005b) Eurocode 3: Design of steel structures-Part 1–1: general rules and rules for buildings. Eur Comm Stand Bruss

CEN (2005c) Eurocode 3: design of steel structures—part 1–8: design of joints—the European standard EN 1993-1-8: 2005. In: European committee for standardization, brussels

CEN (2005d) Eurocode 4. Design of composite steel and concrete structures. Part 1.1: general rules and rules for buildings. Eur Comm Stand Bruss
Chen S-J, Chao YC (2001) Effect of composite action on seismic performance of steel moment connections with reduced beam sections. J Constr Steel Res 57:417–434
Chen S-J, Tsao YC, Chao YC (2001) Enhancement of ductility of existing seismic steel moment connections. J Struct Eng 127:538–545
Chiniforush AA, Ataei A, Bradford MA (2021) Experimental study of deconstructable bolt shear connectors subjected to cyclic loading. J Constr Steel Res 183:106741
Chung KF, Liu TCH, Ko ACH (2001) Investigation on Vierendeel mechanism in steel beams with circular web openings. J Constr Steel Res 57:467–490
Chung KF, Liu CH, Ko ACH (2003) Steel beams with large web openings of various shapes and sizes: an empirical design method using a generalised moment-shear interaction curve. J Constr Steel Res 59:1177–1200
Civjan SA, Engelhardt MD, Gross JL (2000) Retrofit of pre-Northridge moment-resisting connections. J Struct Eng 126:445–452
Civjan SA, Engelhardt MD, Gross JL (2001) Slab effects in SMRF retrofit connection tests. J Struct Eng 127:230–237
Davarpanah M, Ronagh H, Memarzadeh P, Behnamfar F (2020) Cyclic behavior of welded elliptical-shaped RWS moment frame. J Constr Steel Res 175:106319
Davison B, Owens GW (eds) (2012) Steel designers' manual. Wiley, New Jersey
Di Benedetto S, Francavilla AB, Latour M et al (2020) Pseudo-dynamic testing of a full-scale two-storey steel building with RBS connections. Eng Struct 212:110494
Dong Y, Jia L, Xu F, Li X (2021) Experimental study on seismic behavior of steel structure with cellular beams and composite concrete slab. Structures 34:507–522. https://doi.org/10.1016/j.istruc.2021.07.081
Du H, Hu X, Shi D, Fang B (2021) Effect of reinforcement on the strength of the web opening in steel-concrete composite beam. Eng Struct 235:112038. https://doi.org/10.1016/j.engstruct.2021.112038
Erfani S, Akrami V (2017) Increasing seismic energy dissipation of steel moment frames using reduced web section (RWS) connection. J Earthq Eng 21:1090–1112
Erfani S, Akrami V, Mohammad-nejad A (2020) Lateral load resisting behavior of steel moment frames with reduced web section (RWS) beams. Structures. Elsevier, Amsterdam, pp 251–265
Girão Coelho A, Coelho G, Lawson M et al (2020) Guidance on demountable composite construction systems for UK practice. SCI, Berkshire
Jia L, Li Q, Bi R, Dong Y (2021) Behaviour of castellated beam-to-column end-plate connection under monotonic load. Structures 34:4616–4633. https://doi.org/10.1016/j.istruc.2021.10.064
Jones SL, Fry GT, Engelhardt MD (2002) Experimental evaluation of cyclically loaded reduced beam section moment connections. J Struct Eng 128:441–451
Kim Y-J, Oh S-H, Moon T-S (2004) Seismic behavior and retrofit of steel moment connections considering slab effects. Eng Struct 26:1993–2005
Lagaros ND, Psarras LD, Papadrakakis M, Panagiotou G (2008) Optimum design of steel structures with web openings. Eng Struct 30:2528–2537
Landolfo R (2022) European seismic prequalification of steel beam-to-column joints: EQUALJOINTS and EQUALJOINTS-plus projects. J Constr Steel Res 192:107238. https://doi.org/10.1016/j.jcsr.2022.107238
Lawson RM, Hicks SJ (2011) Design of composite beams with large web openings. SCI P355
Lee CH, Jung JH, Kim SY, Kim JJ (2016) Investigation of composite slab effect on seismic performance of steel moment connections. J Constr Steel Res 117:91–100
Lin S, Qiao H, Wang J et al (2021) Anti-collapse performance of steel frames with RWS connections under a column removal scenario. Eng Struct 227:111495
Lin S, Xue X, Qiao H, Chen Y (2022) Prediction model for catenary action of welded RWS connections using PVM link element. J Constr Steel Res 191:107207
Liu TCH, Chung KF (2003) Steel beams with large web openings of various shapes and sizes: finite element investigation. J Constr Steel Res 59:1159–1176
Liu X, Bradford MA, Ataei A (2017) Flexural performance of innovative sustainable composite steel-concrete beams. Eng Struct 130:282–296. https://doi.org/10.1016/j.engstruct.2016.10.009
Moynihan MC, Allwood JM (2014) Viability and performance of demountable composite connectors. J Constr Steel Res 99:47–56. https://doi.org/10.1016/j.jcsr.2014.03.008
Roeder CW (2002) Connection performance for seismic design of steel moment frames. J Struct Eng 128:517–525

Sencu RM, Wang YC, Yang J, Lam D (2019) Performance evaluation of demountable shear connectors with collar step at ambient and elevated temperatures. Eng Struct 194:94–105. https://doi.org/10.1016/j.engstruct.2019.05.059

Shaheen MA, Tsavdaridis KD, Yamada S (2018) Comprehensive FE study of the hysteretic behaviour of steel-concrete composite and non-composite RWS beam-to-column connections. J Struct Eng 144:04018150

Shin M, Kim S-P, Halterman A, Aschheim M (2017a) Seismic toughness and failure mechanisms of reduced web-section beams: phase 2 tests. Eng Struct 141:607–623

Shin M, Kim S-P, Halterman A, Aschheim M (2017b) Seismic toughness and failure mechanisms of reduced web-section beams: phase 1 tests. Eng Struct 141:198–216

Sumner EA, Murray TM (2002) Behavior of extended end-plate moment connections subject to cyclic loading. J Struct Eng 128:501–508

Tabar AM, Alonso-Rodriguez A, Tsavdaridis KD (2022) Building retrofit with reduced web (RWS) and beam (RBS) section limited-ductility connections. J Constr Steel Res 197:107459

Tartaglia R, D'Aniello M, Rassati GA (2019) Proposal of AISC-compliant seismic design criteria for ductile partially-restrained end-plate bolted joints. J Constr Steel Res 159:364–383

Tsavdaridis KD, D'Mello C (2012) Vierendeel bending study of perforated steel beams with various novel web opening shapes through nonlinear finite-element analyses. J Struct Eng 138:1214–1230

Tsavdaridis KD, Papadopoulos T (2016) A FE parametric study of RWS beam-to-column bolted connections with cellular beams. J Constr Steel Res 116:92–113

Tsavdaridis KD, Faghih F, Nikitas N (2014) Assessment of perforated steel beam-to-column connections subjected to cyclic loading. J Earthq Eng 18:1302–1325

Tsavdaridis KD, Pilbin C, Lau CK (2017) FE parametric study of RWS/WUF-B moment connections with elliptically-based beam web openings under monotonic and cyclic loading. Int J Steel Struct 17:677–694

Tsavdaridis KD, Lau CK, Alonso-Rodríguez A (2021) Experimental behaviour of non-seismical RWS connections with perforated beams under cyclic actions. J Constr Steel Res 183:106756

Yang Q, Li B, Yang N (2009) Aseismic behaviors of steel moment resisting frames with opening in beam web. J Constr Steel Res 65:1323–1336

Yang F, Liu Y, Jiang Z, Xin H (2018) Shear performance of a novel demountable steel-concrete bolted connector under static push-out tests. Eng Struct 160:133–146. https://doi.org/10.1016/j.engstruct.2018.01.005

Zhang X, Ricles JM (2006a) Experimental evaluation of reduced beam section connections to deep columns. J Struct Eng 132:346–357

Zhang X, Ricles JM (2006b) Seismic behavior of reduced beam section moment connections to deep columns. J Struct Eng 132:358–367

Zhang X, Zheng S, Zhao X (2019) Seismic performance of steel beam-to-column moment connections with different structural forms. J Constr Steel Res 158:130–142

Publisher's Note Springer Nature remains neutral with regard to jurisdictional claims in published maps and institutional affiliations.